The Yeoh model applied to the modeling of large deformation contact/impact problems

Christine Renaud, Jean-Michel Cros, Zhi-Qiang Feng, Bintang Yang

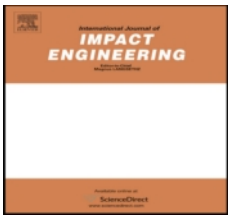

Title: The Yeoh model applied to the modeling of large deformation contact/impact problems

Authors: Christine Renaud, Jean-Michel Cros, Zhi-Qiang Feng, Bintang Yang

PII: S0734-743X(08)00235-2
DOI: 10.1016/j.ijimpeng.2008.09.008
Reference: IE 1707

To appear in: *International Journal of Impact Engineering*

Received Date: 31 January 2008
Revised Date: 5 September 2008
Accepted Date: 22 September 2008

Please cite this article as: Renaud C, Cros JM, Feng ZQ, Yang B. The Yeoh model applied to the modeling of large deformation contact/impact problems, International Journal of Impact Engineering (2008), doi: 10.1016/j.ijimpeng.2008.09.008

The Yeoh model applied to the modeling of large deformation contact/impact problems

Christine Renaud [a], Jean-Michel Cros [a], Zhi-Qiang Feng [a,*], Bintang Yang [b]

[a] *Laboratoire de Mécanique d'Évry, Université d'Évry-Val d'Essonne 40 rue du Pelvoux, 91020 Évry, France*

[b] *School of Mechanical Engineering, Shanghai Jiaotong University 800 Dongchuan Road, Min Hang, 200240 Shanghai, China*

Abstract

The present paper is devoted to the modeling of finite deformations of hyperelastic bodies described by the Yeoh model under contact/impact conditions. A total Lagrangian formulation is adopted to describe the geometrically nonlinear behavior. A first order algorithm is applied to integrate the equations of motion. For the finite element implementation, an explicit expression of the tangent operator is derived. Two numerical examples are presented to show the applicability of the developed approach.

Key words: Hyperelasticity, Contact/Impact, Large deformation

1 Introduction

Problems involving contact and friction are among the most difficult ones to solve in mechanics and at the same time of practical importance in many engineering branches. A large number of algorithms for the modeling of contact problems by the finite element method have been presented in the literature. See for example the monographs by Wriggers [1] and Laursen [2] and the references therein. De Saxcé and Feng [3] have proposed a bi-potential method combined with an augmented Lagrangian formulation. Feng *et al.* [4] have

* Tel.: +33 1 69 47 75 01; Fax: +33 1 69 47 75 99.
E-mail address: feng@iup.univ-evry.fr

successfully applied this method to the modeling of static contact problems between Blatz-Ko hyperelastic bodies.

Regarding the time integration for implicit dynamic analysis in structural mechanics, the most commonly used scheme is the second order scheme such as Newmark, Wilson-θ, HHT [5]. A first order time scheme has also been proposed by Jean [6] for time stepping in granular mechanics. Recently, Feng *et al.* [7,8] have applied this scheme for the modeling of impact problems between elastic bodies.

In nonlinear elasticity, there exist many constitutive models describing the hyperelastic behavior of foam-like or rubber-like materials [9–15]. These models are available in many modern commercial finite element codes. The aim of the present paper is to propose a finite element implementation of the Yeoh model, in view of application to contact/impact problems involving large displacements and large deformations.

2 Hyperelastic bodies and the Yeoh model

Rubber-like materials are usually taken to be hyperelastic and often undergo large deformations. To describe the geometrical transformations in $\mathbb{R}^3$, the deformation gradient tensor is introduced by

$$\mathbf{F} = \mathbf{I} + \frac{\partial \mathbf{u}}{\partial \mathbf{X}} \quad \text{with} \quad J = \det(\mathbf{F}) > 0\,, \tag{1}$$

where $\mathbf{I}$ is the identity tensor, $\mathbf{X} \in \mathbb{R}^3$ the reference position vector and $\mathbf{u} \in \mathbb{R}^3$ the displacement vector. The right Cauchy-Green strain tensor $\mathbf{C}$ and the Green-Lagrange strain tensor $\mathbf{E}$ are defined as

$$\mathbf{C} = \mathbf{F}^{\mathrm{T}}\mathbf{F}\,, \quad \mathbf{E} = \frac{1}{2}(\mathbf{C} - \mathbf{I})\,. \tag{2}$$

For a hyperelastic law, there exists an elastic potential function W (or strain energy density function) which is a scalar function of one of the strain tensors. Differentiation of W with respect to the Green strain gives the energy conjugate second Piola-Kirchoff stress $\mathbf{S}$:

$$\mathbf{S} = \frac{\partial W}{\partial \mathbf{E}} = 2\frac{\partial W}{\partial \mathbf{C}}\,. \tag{3}$$

The Yeoh model (called also the third-order reduced polynomial form) describes isotropic incompressible rubber-like materials [12]. The strain energy

potential is given by

$$W(I_1) = \sum_{i=1}^{3} C_{i0}(I_1 - 3)^i. \tag{4}$$

One particularity of this model is that it depends only on the first strain invariant $I_1 = tr(\mathbf{C})$. It applies to the characterization of elastic properties of carbon-black filled rubber vulcanizates. It has been demonstrated to fit various modes of deformation using the data obtained from a uniaxial tension test only. This leads to reduced requirements on material testing.

For numerical purpose, it proves useful to separate the deformation in volumetric and isochoric parts by a multiplicative split of a deformation gradient as

$$\mathbf{F} = \mathbf{F}^{iso}\mathbf{F}^{vol}, \quad \text{with} \quad \mathbf{F}^{vol} = J^{1/3}\mathbf{I}, \quad \mathbf{F}^{iso} = J^{-1/3}\mathbf{F}\,. \tag{5}$$

This decomposition is such that $\det(\mathbf{F}^{iso}) = 1$. It is easy to see that $\mathbf{F}$ and $\mathbf{F}^{iso}$ have the same eigenvectors. The isochoric part of the right Cauchy-Green strain tensor $\mathbf{C}$ can be then defined as

$$\mathbf{C}^{iso} = J^{-2/3}\mathbf{C}\,. \tag{6}$$

The first strain invariant of $\mathbf{C}^{iso}$ is then defined by $\overline{I_1} = J^{-2/3}I_1$ which replaces I_1 in $W(I_1)$. In order to enforce the incompressibility constraint, another term is also added so as to obtain finally the following strain energy function:

$$W(\overline{I_1}, J) = \sum_{i=1}^{3} C_{i0}(\overline{I_1} - 3)^i + \sum_{k=1}^{3} \frac{1}{d_k}(J-1)^{2k}\,, \tag{7}$$

where C_{i0} and d_k are material constants. By expressing the strain energy density in terms of the invariants of the right Cauchy-Green strain tensor, Eq.(3) becomes

$$\begin{aligned}\mathbf{S} = & 2\left(\sum_{i=1}^{3} iC_{i0}(\overline{I_1} - 3)^{i-1}\right) J^{-\frac{2}{3}}\left[\mathbf{I} - \frac{I_1}{3}\mathbf{C}^{-1}\right] \\ & + \left(\sum_{k=1}^{3} \frac{2k}{d_k}(J-1)^{2k-1}\right)\, J\,\mathbf{C}^{-1}\,.\end{aligned} \tag{8}$$

The Cauchy stress (or true stress) tensor $\boldsymbol{\sigma}$ is calculated from the second Piola-Kirchoff stress tensor $\mathbf{S}$:

$$\boldsymbol{\sigma} = \frac{1}{J}\mathbf{F}\mathbf{S}\mathbf{F}^{\mathrm{T}}\,. \tag{9}$$

To construct the tangent stiffness matrix for the analysis of nonlinear structures by the finite element method, one has to determine the stress-strain tangent operator $\mathbb{D}$, which is a fourth-order tensor resulting from the derivation of $\mathbf{S}$ with respect to $\mathbf{E}$ in Eq.(8):

$$\begin{aligned}\mathbb{D} = & 4J^{-\frac{4}{3}}\alpha\left[\mathbf{I}-\frac{I_1}{3}\mathbf{C}^{-1}\right]\otimes\left[\mathbf{I}-\frac{I_1}{3}\mathbf{C}^{-1}\right] \\ & -\frac{4}{3}J^{-\frac{2}{3}}\beta\left[\mathbf{C}^{-1}\otimes\mathbf{I}+\mathbf{I}\otimes\mathbf{C}^{-1}-\frac{I_1}{3}\mathbf{C}^{-1}\otimes\mathbf{C}^{-1}-I_1\ \mathbf{C}^{-1}\overline{\underline{\otimes}}\mathbf{C}^{-1}\right] \\ & +\gamma\ J^2\ \mathbf{C}^{-1}\otimes\mathbf{C}^{-1}+\delta\ J\ \left[\mathbf{C}^{-1}\otimes\mathbf{C}^{-1}-2\mathbf{C}^{-1}\overline{\underline{\otimes}}\mathbf{C}^{-1}\right]. \end{aligned} \tag{10}$$

where

$$\begin{aligned}\alpha &= \sum_{i=2}^{3} i(i-1)\ C_{i0}(\overline{I_1}-3)^{i-2}, \quad \beta = \sum_{i=1}^{3} i\ C_{i0}(\overline{I_1}-3)^{i-1}, \\ \gamma &= \sum_{k=1}^{3}\frac{2k(2k-1)}{d_k}(J-1)^{2k-2}, \quad \delta = \sum_{k=1}^{3}\frac{2k}{d_k}(J-1)^{2k-1}.\end{aligned}$$

The coordinate-free symbols $\otimes$ and $\overline{\underline{\otimes}}$ used above are related to the corresponding index symbols in the following way:

$$(\mathbf{A}\otimes\mathbf{B})_{ijkl} = A_{ij}B_{kl}, \quad (\mathbf{A}\,\overline{\underline{\otimes}}\,\mathbf{B})_{ijkl} = \frac{1}{2}\left(A_{ik}B_{jl}+A_{il}B_{jk}\right). \tag{11}$$

3 Finite element formulation

3.1 Equations of motion

In the case of dynamic multibody contact problems with large deformations of hyperelastic solids, the nonlinear relationship between strains and displacements cannot be ignored. The total Lagrangian formulation is adopted in this work to describe nonlinear behavior. It is well known that the strain tensor $\mathbf{E}$ and the stress tensor $\mathbf{S}$ are both symmetric. Thus, we note hereafter $\mathbf{E}$ and $\mathbf{S}$ in vector form as

$$\begin{aligned}\mathbf{E} &= \left\langle\ E_{11}\ E_{22}\ E_{33}\ 2E_{12}\ 2E_{13}\ 2E_{23}\ \right\rangle^{\mathrm{T}}, \\ \mathbf{S} &= \left\langle\ S_{11}\ S_{22}\ S_{33}\ S_{12}\ S_{13}\ S_{23}\ \right\rangle^{\mathrm{T}}.\end{aligned} \tag{12}$$

In the context of the finite element method and with Eq.(1) and Eq.(2), the Green-Lagrange strain can be formally written with linear and nonlinear contributions in terms of nodal displacements [14]:

$$\mathbf{E} = \Big(\mathbf{B}_L + \frac{1}{2}\mathbf{B}_{NL}(\mathbf{u})\Big)\mathbf{u}\,, \tag{13}$$

where $\mathbf{B}_L$ is the matrix which relates the linear part of the strain term to the nodal displacements, and $\mathbf{B}_{NL}(\mathbf{u})$, the matrix which relates the nonlinear strain term to the nodal displacements. From Eq.(13), the incremental form of the strain-displacement relationship is

$$\delta\mathbf{E} = \Big(\mathbf{B}_L + \mathbf{B}_{NL}(\mathbf{u})\Big)\delta\mathbf{u}\,. \tag{14}$$

Without going into detail, nonlinear dynamic contact problems can be governed by the following equations of motion:

$$\mathbf{M}\ddot{\mathbf{u}} + \mathbf{A}\dot{\mathbf{u}} + \mathbf{F}_{int} - \mathbf{F}_{ext} - \mathbf{R} = 0\,. \tag{15}$$

where $\mathbf{F}_{ext}$ is the vector of external loads, $\mathbf{R}$ the contact reaction vector, $\mathbf{M}$ the mass matrix, $\mathbf{A}$ the damping matrix, $\dot{\mathbf{u}}$ the velocity vector and $\ddot{\mathbf{u}}$ the acceleration vector. The vector of internal forces is defined by

$$\mathbf{F}_{int} = \int_{V_0} \Big(\mathbf{B}_L + \mathbf{B}_{NL}(\mathbf{u})\Big)^{\mathrm{T}}\mathbf{S}\,dV\,, \tag{16}$$

where V_0 is the domain of the initial configuration.

Equation (15) can be transformed to

$$\mathbf{M}\,\ddot{\mathbf{u}} = \mathbf{F} + \mathbf{R}, \quad \mathbf{F} = \mathbf{F}_{ext} - \mathbf{F}_{int} - \mathbf{A}\dot{\mathbf{u}}\,, \tag{17}$$

to be solved with the initial conditions at $t = 0$,

$$\dot{\mathbf{u}} = \dot{\mathbf{u}}_0 \text{ and } \mathbf{u} = \mathbf{u}_0\,. \tag{18}$$

Taking the derivative of $\mathbf{F}_{int}$ with respect to the nodal displacements $\mathbf{u}$ yields the tangent stiffness matrix:

$$\mathbf{K} = \frac{\partial \mathbf{F}_{int}}{\partial \mathbf{u}} = \mathbf{K}_e + \mathbf{K}_\sigma + \mathbf{K}_u\,, \tag{19}$$

where $\mathbf{K}_e$, $\mathbf{K}_\sigma$ and $\mathbf{K}_u$ stand respectively for the elastic stiffness matrix, the geometric stiffness (or initial stress stiffness) matrix and the initial displacement stiffness matrix:

$$\mathbf{K}_e = \int_{V_0} \mathbf{B}_L^{\mathrm{T}}\mathbf{D}\mathbf{B}_L\,dV\,, \tag{20}$$

$$\mathbf{K}_\sigma = \int_{V_0} \frac{\partial \mathbf{B}_{NL}^{\mathrm{T}}}{\partial \mathbf{u}}\,\mathbf{S}\,dV\,, \tag{21}$$

$$\mathbf{K}_u = \int_{V_0} \left(\mathbf{B}_L^{\mathrm{T}} \mathbf{D} \mathbf{B}_{NL} + \mathbf{B}_{NL}^{\mathrm{T}} \mathbf{D} \mathbf{B}_L + \mathbf{B}_{NL}^{\mathrm{T}} \mathbf{D} \mathbf{B}_{NL} \right) dV \,. \tag{22}$$

where $\mathbf{D}$ denotes the usual material tangent matrix, deduced from the stress-strain tangent operator $\mathbb{D}$ (Eq.(10)) due to its major and minor symmetry.

3.2 First order time integration

Equation (17) has to be integrated between consecutive time configurations at time t and $t + \Delta t$. Usually a Newmark scheme based on a second order approximation is used. However, in impact problems, this scheme may lead to no physical energy oscillation and no stable solution as shown in the second numerical example of this paper. These phenomena are also discussed in [2,16]. At the moment of a sudden change of contact conditions (impact, release of contact), the velocity and acceleration are not continuous in time, and excessive regularity of constraints may lead to errors. For this reason, Jean [6] proposed a first order time scheme which is used in this work. This scheme is based on the following approximations:

$$\int_t^{t+\Delta t} \mathbf{M}\, d\dot{\mathbf{u}} = \mathbf{M} \left(\dot{\mathbf{u}}^{t+\Delta t} - \dot{\mathbf{u}}^t \right) , \tag{23}$$

$$\int_t^{t+\Delta t} \mathbf{F}\, dt = \Delta t \left((1-\xi)\, \mathbf{F}^t + \xi\, \mathbf{F}^{t+\Delta t} \right) , \tag{24}$$

$$\int_t^{t+\Delta t} \mathbf{R}\, dt = \Delta t\, \mathbf{R}^{t+\Delta t} , \tag{25}$$

$$\mathbf{u}^{t+\Delta t} - \mathbf{u}^t = \Delta t \left((1-\theta)\, \dot{\mathbf{u}}^t + \theta\, \dot{\mathbf{u}}^{t+\Delta t} \right) , \tag{26}$$

with the parameters $0 \leq \xi, \theta \leq 1$. The transient integration parameter θ defaults to 0.5 (Crank-Nicholson method). If $\theta = 1$, the method is referred to as the backward Euler method. For all $\theta > 0$, the system equations that follow are said to be implicit. In addition, for the more limiting case of $\theta \geq 0.5$, the solution of these equations is said to be unconditionally stable.

In the iterative solution procedure, all the values at time $t + \Delta t$ are replaced by the values of the current iteration $i + 1$; for example, $\mathbf{F}^{t+\Delta t} = \mathbf{F}^{i+1}$. A standard approximation of $\mathbf{F}^{i+1}$ is

$$\begin{aligned} \mathbf{F}^{i+1} &= \mathbf{F}_{int}^i + \frac{\partial \mathbf{F}}{\partial \mathbf{u}} (\mathbf{u}^{i+1} - \mathbf{u}^i) + \frac{\partial \mathbf{F}}{\partial \dot{\mathbf{u}}} (\dot{\mathbf{u}}^{i+1} - \dot{\mathbf{u}}^i) \\ &= \mathbf{F}_{int}^i - \mathbf{K}^i\, \Delta \mathbf{u} - \mathbf{A}^i\, \Delta \dot{\mathbf{u}} \,. \end{aligned} \tag{27}$$

Finally, we obtain the recursive form of Eq.(17) in terms of displacements:

$$\begin{aligned} \bar{\mathbf{K}}^i \, \Delta\mathbf{u} &= \bar{\mathbf{F}}^i + \bar{\mathbf{F}}^i_{acc} + \mathbf{R}^{i+1} \,, \\ \mathbf{u}^{i+1} &= \mathbf{u}^i + \Delta\mathbf{u} \,, \end{aligned} \tag{28}$$

where the so-called effective terms are given by

$$\bar{\mathbf{K}}^i = \xi \, \mathbf{K}^i + \frac{\xi}{\theta \, \Delta t}\mathbf{A}^i + \frac{1}{\theta \, \Delta t^2}\mathbf{M}^i \,, \tag{29}$$

$$\bar{\mathbf{F}}^i_{acc} = -\frac{1}{\theta \Delta t^2} \, \mathbf{M}^i \left\{ \mathbf{u}^i - \mathbf{u}^t - \Delta t \, \dot{\mathbf{u}}^t \right\} \,, \tag{30}$$

$$\bar{\mathbf{F}}^i = (1-\xi) \left(\mathbf{F}^t_{int} + \mathbf{F}^t_{ext} \right) + \xi \left(\mathbf{F}^i_{int} + \mathbf{F}^{t+\Delta t}_{ext} \right) \,. \tag{31}$$

To complete the time step, the velocity is updated according to

$$\dot{\mathbf{u}}^{t+\Delta t} = \left(1 - \frac{1}{\theta} \right) \dot{\mathbf{u}}^t + \frac{1}{\theta \, \Delta t} (\mathbf{u}^{t+\Delta t} - \mathbf{u}^t) \,. \tag{32}$$

Equation (28) is strongly non-linear, because of large rotations and large deformations involved. Besides, in multibody contact/impact problems, unilateral contact and friction, characterized by inequalities, are non-smooth phenomena. To solve this equation instead of considering all nonlinearities at the same time, a strategy was proposed in [17] which consists in separating the nonlinearities so as to overcome the complexity of calculation and to improve the numerical stability. As $\Delta\mathbf{u}$ and $\mathbf{R}$ are both unknown, Eq.(28) cannot be directly solved. First, the vector $\mathbf{R}$ is determined using the bi-potential method in a reduced system, involving only contact nodes. The reader can refer to [3,4,17] for more details on the bi-potential method. Then, the vector $\Delta\mathbf{u}$ is computed over the whole structure, using contact reactions as external loadings. It is important to note that, as opposed to the penalty method or Lagrange multiplier method, the bi-potential method neither changes the global stiffness matrix nor increases the number of degrees of freedom. This interesting feature makes it easy to implement contact and friction problems in existing general-purpose finite element codes. In addition, the solution procedure is more stable because of the separation of nonlinearities and improved numerical algorithms for calculation of contact reactions.

4 Numerical results

The algorithm presented above (named Bi-First) has been implemented in the finite element code FER/Impact [18]. To illustrate the results of the contact/impact simulation using the Bi-First algorithm, we consider here two examples.

4.1 Two-dimensional static contact

The first example studied concerns the indentation of a rigid circular cylinder into an hyperelastic body relying on a rigid foundation. The radius of cylinder is 50 mm. The dimension of the deformable body is 280 × 80 mm. The Yeoh model is considered and the material constants are: $C_{10} = 0.235$ MPa, $C_{20} = -0.007$ MPa, $C_{30} = 0.0008$ MPa, $d_1 = d_2 = d_3 = 0.1$. These values correspond to a silicon material. The finite element discretization includes 445 four-node isoparametric plane strain elements and 506 nodes. Thirty load steps are performed for this problem and a vertical displacement of 1 mm is applied to the cylinder each step. Two coefficients of Coulomb friction are used: $\mu = 0.4$ between the cylinder and the body, $\mu = 0.1$ between the body and the foundation. Figure 1 shows the initial mesh and two computed deformed configurations when the applied displacements are equal to 15 and 30 mm. Figure 2 shows the distribution of the von-Mises stress. When the friction between the body and the foundation increases slightly ($\mu = 0.2$), the stress concentration is moved slightly towards to cylinder as shown in Figure 3. It is worth noting that the stress concentration is located inside the body rather than on the boundary. Moreover, under the contact loading of the cylinder, the body is partially separated from the foundation. The contact zone between the cylinder and body is refined which allows for a better representation of contact conditions (Figure 4). Figure 5 gives the evolution of applied load with respect to the controlled displacement of the cylinder. The influence of friction effects is obvious, only after 10 load steps.

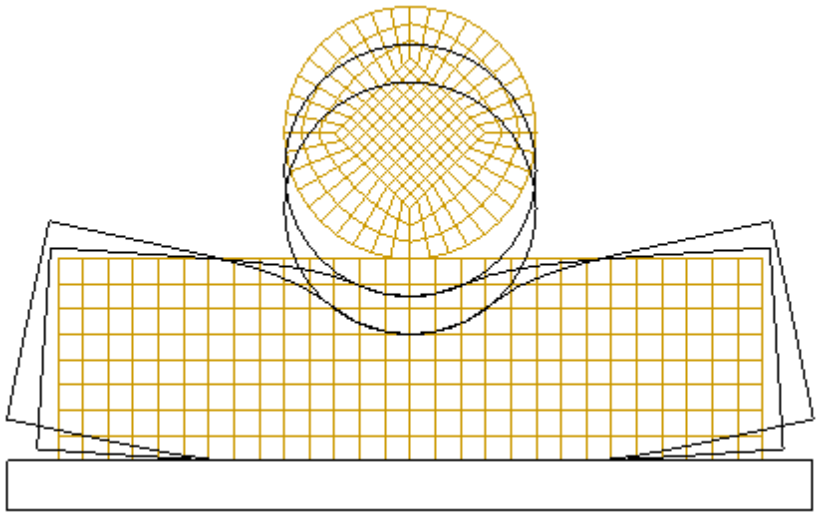

Fig. 1. Initial mesh and deformed outlines

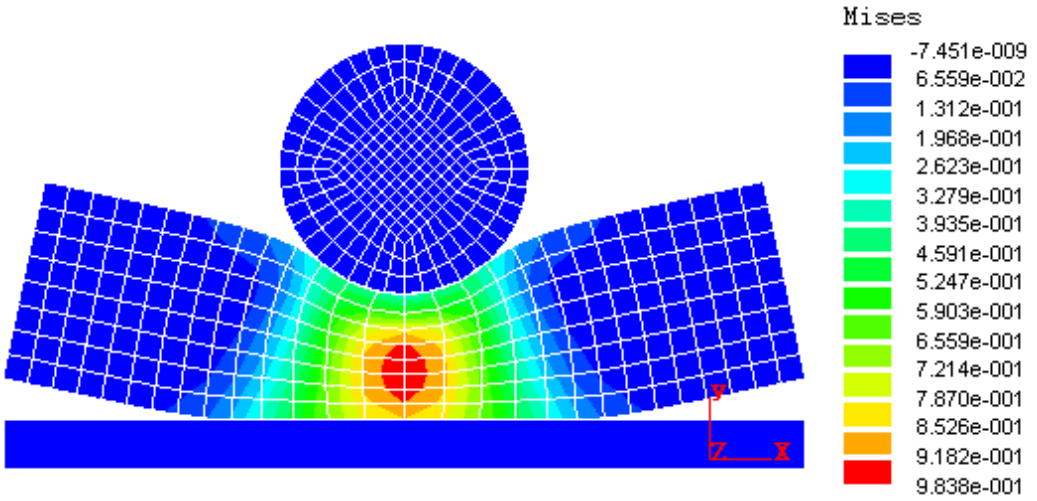

Fig. 2. Distribution of von-Mises stress ($\mu = 0.1$)

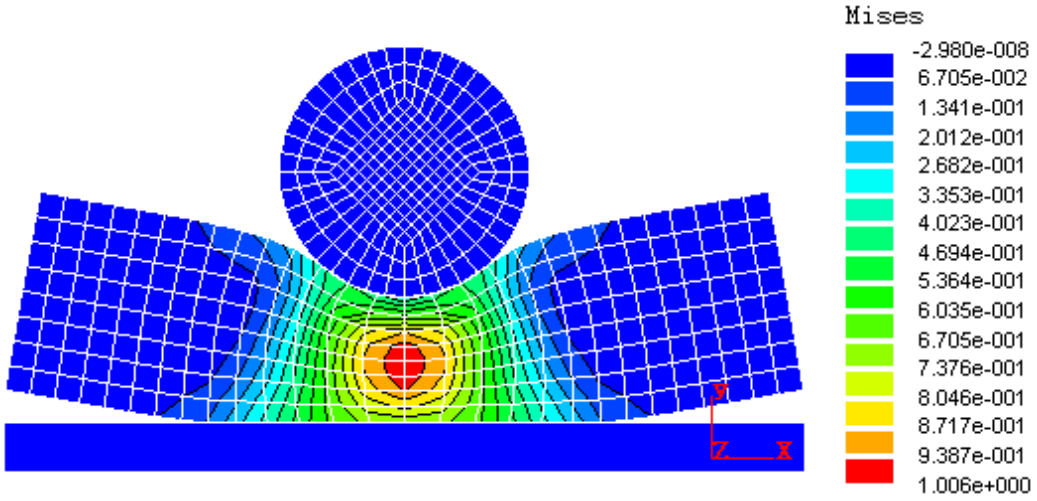

Fig. 3. Distribution of von-Mises stress ($\mu = 0.2$)

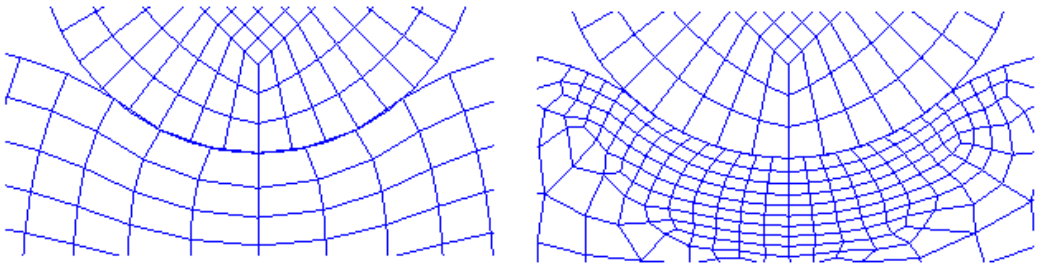

Fig. 4. Refined mesh at contact region

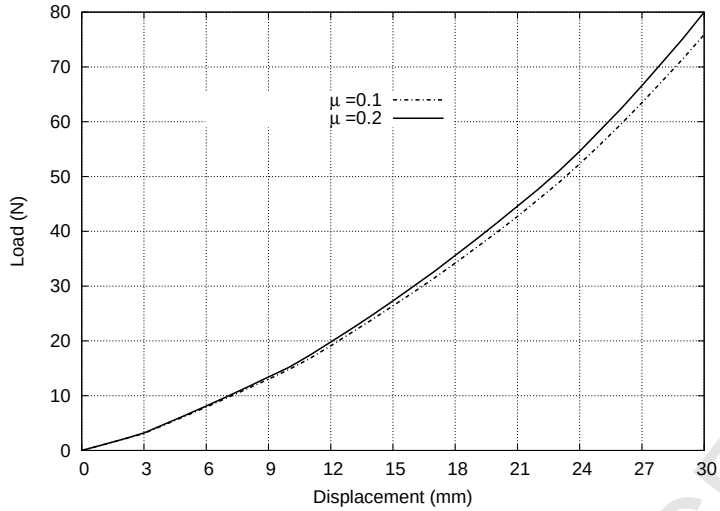

Fig. 5. Load versus displacement: influence of friction coefficient

As a comparison, we also use the general purpose finite element program ANSYS for analysis of the same problem. Figure 6 shows the vertical displacement u_y of contact nodes between the body and the foundation corresponding to the last load step. It demonstrates that our approach allows to satisfy accurately the contact impenetrability condition, but it is not the case with ANSYS. Figure 7 depicts the load-displacement curves. The difference can be explained by the penetration between the contact surfaces in the ANSYS solution.

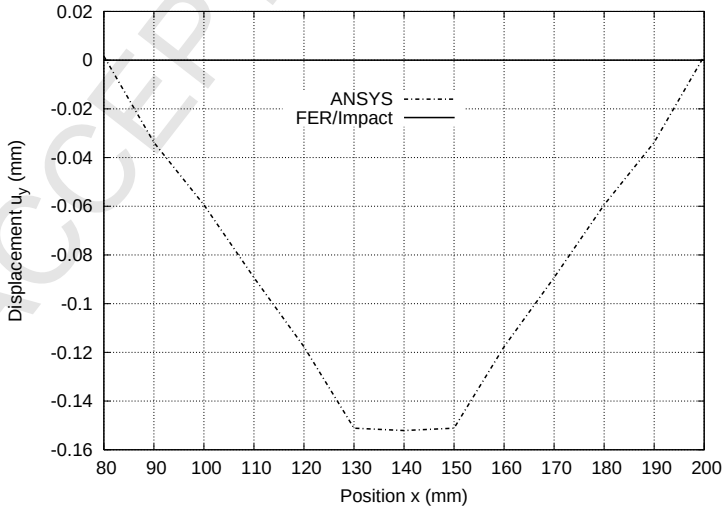

Fig. 6. Penetration: comparison between ANSYS and FER/Impact

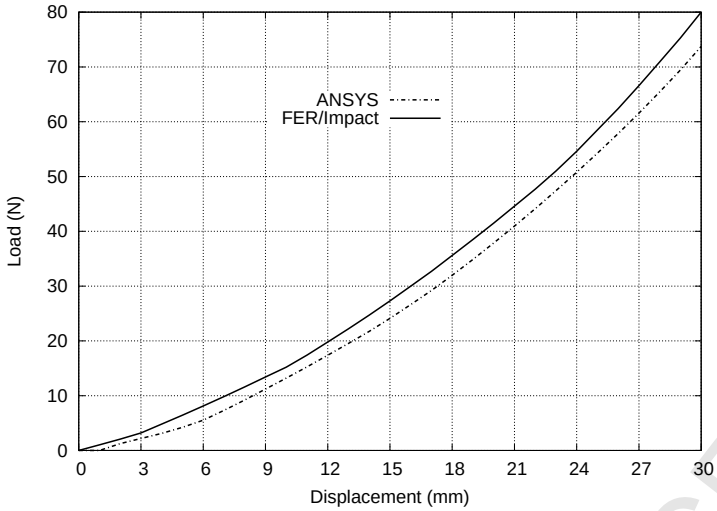

Fig. 7. Load versus displacement: comparison between ANSYS and FER/Impact

4.2 Three-dimensional dynamic contact

The problem consists of two three-dimensional hyperelastic blocks (Figure 8) one impacting the other with relative tangential motion.

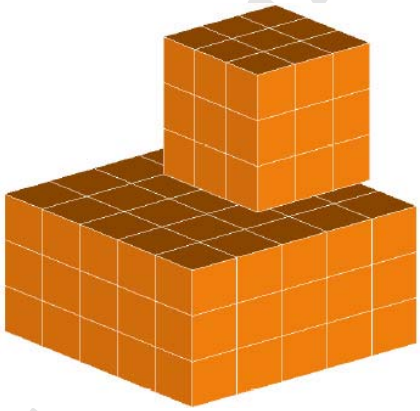

Fig. 8. Initial configuration and mesh

Normalized units are used in this example. The base of the larger block is fixed, and the smaller block has an initial rigid-body velocity of $\{0.0, 2.0, -1.0\}$ that initiates a glancing impact. The larger block initially occupies the cubic space defined by diagonal corner points $\{0, 0, 0\}$ and $\{2.0, 2.0, 1.0\}$ and the smaller block is similarly defined by points $\{0.5, 0.0, 1.05\}$ and $\{1.5, 1.0, 2.05\}$. The density is 0.01. The Yeoh model is considered and the parameters of the model are [19]: $C_{10} = 0.3794$, $C_{20} = 0.0232$, $C_{30} = -0.0003$, $d_1 = d_2 = d_3 = 0.01$. The total simulation time is 0.5 scaled time unit and the numerical parameters are: $\Delta t = 0.005$, $\xi = \theta = 0.5$. To investigate the frictional effects on the

energy dissipation, different coefficients of Coulomb friction are used: $\mu = 0.0$ (frictionless), $0.4, 0.8$.

Figures 9 and 10 show the deformed shapes at time $t = 0.07$ and $t = 0.2$ with the friction coefficient $\mu = 0.4$. The isocontours represent the distribution of the von-Mises stress inside the blocks (the maximum value is 0.3821 unit of stress). Similarly, Figures 11 and 12 show the case with $\mu = 0.8$. The maximum value of the von-Mises stress is 0.9823 unit of stress. These plots highlight the impact of the friction coefficient on the stress level and relative slips. The case with $\mu = 0.4$ corresponds a sliding contact status while the case with $\mu = 0.8$ corresponds almost a sticking contact status.

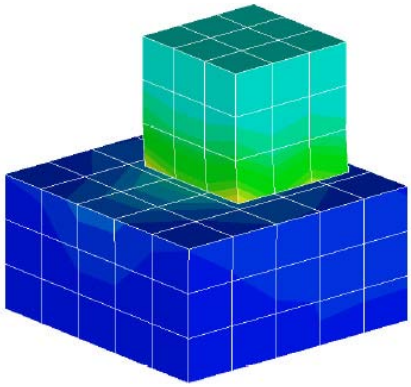

Fig. 9. Deformed shape and von-Mises stress ($\mu = 0.4, t = 0.07$)

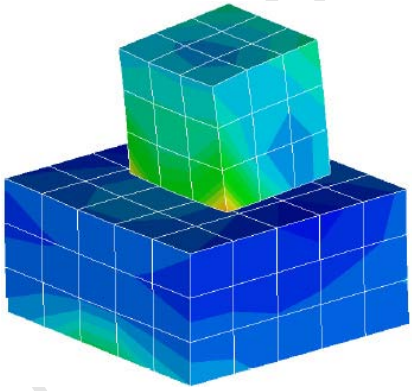

Fig. 10. Deformed shape and von-Mises stress ($\mu = 0.4, t = 0.2$)

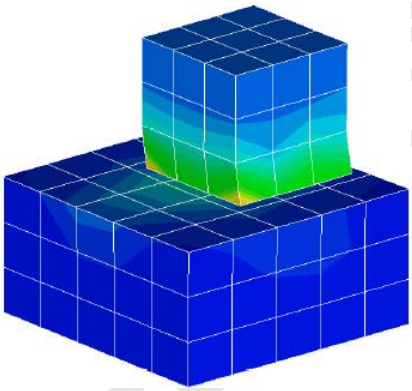

Fig. 11. Deformed shape and von-Mises stress ($\mu = 0.8, t = 0.07$)

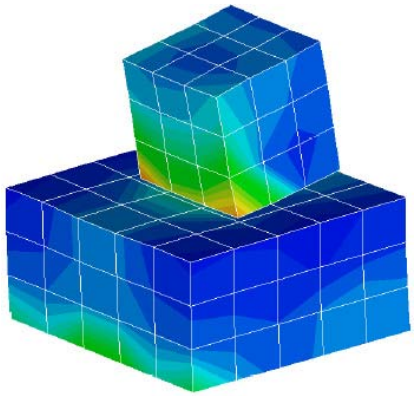

Fig. 12. Deformed shape and von-Mises stress ($\mu = 0.8, t = 0.2$)

Figures 13-15 show the plots of the kinetic energy E_k, the elastic strain energy E_e and the total energy E_t ($E_t = E_k + E_e$) versus time and friction coefficients. We observe that the total energy is quite well conserved in the case of frictionless contact (Figure 15). However, in the case of frictional contact, the total energy decreases. So the total energy is dissipated by frictional effects as expected. It is worth mentioning that the dissipated energy is quantitatively

determined. This result makes it possible to identify numerically the damping and energy restitution coefficients in dynamics problems.

It is also interesting to examine another question: is the dissipated energy proportional to the friction coefficient? The answer is negative according to numerical results. The proof is illustrated in Figure 15 where we observe that the dissipated energy is less for $\mu = 0.8$ than for $\mu = 0.4$. In fact, when the friction coefficient increases, the friction forces increase too. However, the tangential slips decrease. We know that the dissipated energy depends not only on the friction forces but also on the tangential slips on the contact surface.

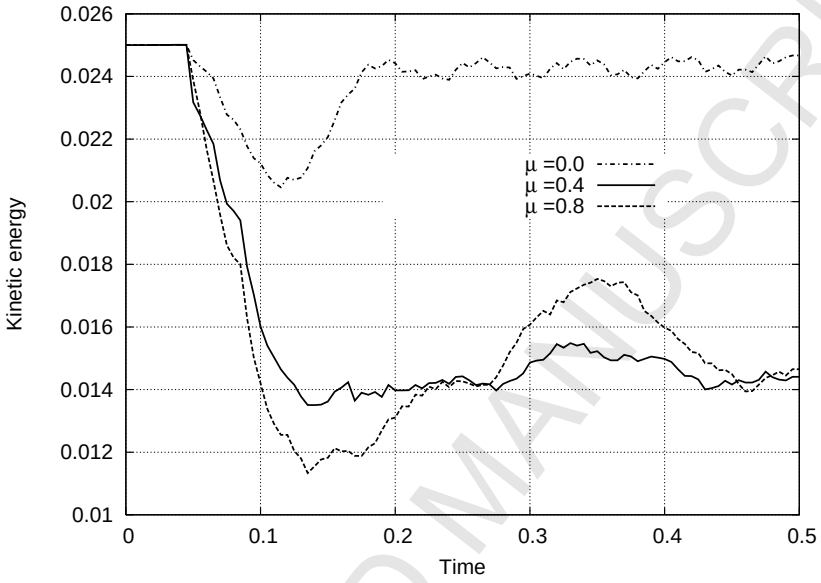

Fig. 13. Kinetic energy with different μ

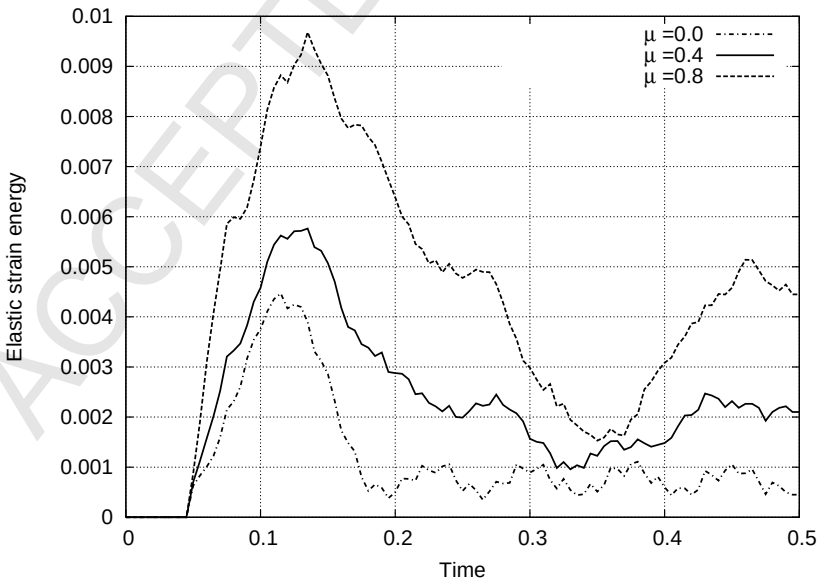

Fig. 14. Strain energy with different μ

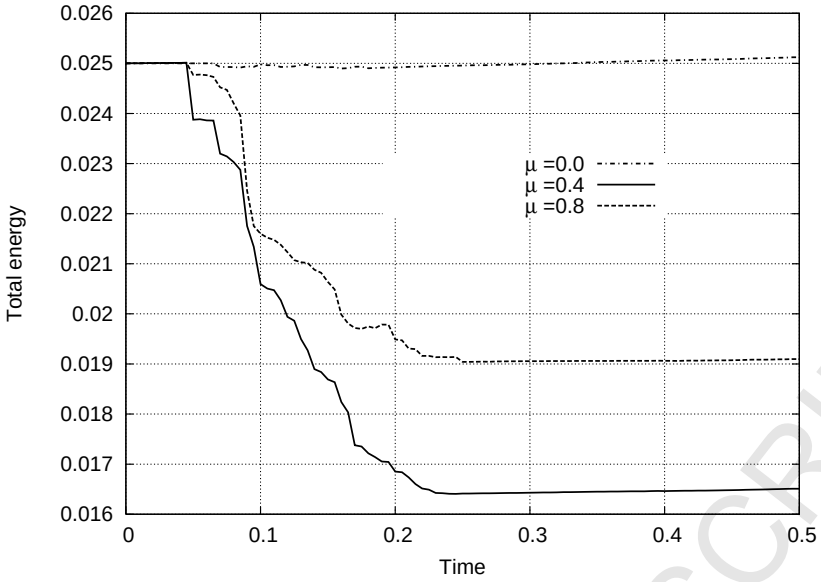

Fig. 15. Total energy with different μ

In order to study the sensitivity of solution with respect to the integration parameter θ, we consider the case of $\mu = 0.0$. Figure 16 shows the evolution of the total energy versus time from which we can see that augmentation of θ leads to more dissipated energy. This dissipation is not physical but numerical. It is obvious that the value of $\theta = 0.5$ allows for a better conservation of energy.

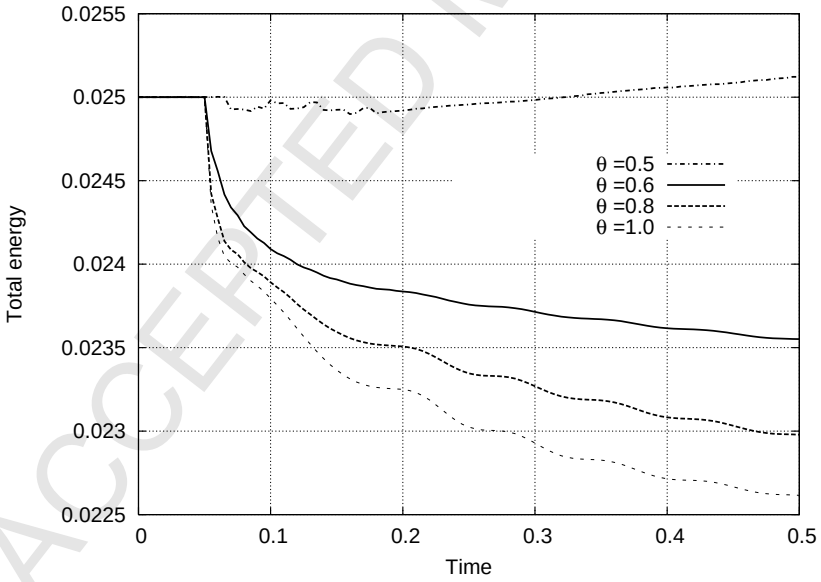

Fig. 16. Influence of the integration parameter θ

For the purpose of comparison, we consider the case of $\mu = 0.4$ and we apply two other time integration methods to solve the equation of motion (Eq.17): the Newmark method and the HHT method [5]. The Newmark integration

parameters are chosen as $\alpha = 0.25$ and $\beta = 0.5$. These values correspond to the trapezoidal rule which is commonly used in elasto-dynamics applications. In the HHT time integration method, a numerical damping is introduced by means of the amplitude decay factor (γ). Chung and Hulbert has shown some interesting property of HHT for the numerical damping [20]. The value $\gamma = 0.1$ is used in this example.

Figure 17 shows the evolution of the total energy versus time. It is observed that both Newmark and HHT methods are much less stable than the present first order time integration method (with $\theta = 0.5$). The HHT method provides similar results as the Newmark method, but with more dissipated energy due to the numerical damping. The performance of the present approach in terms of CPU time, as compared to the Newmark and HHT methods, is reported in Table 1, which shows the efficiency of the proposed method. It is noted that these analyses were performed on a PC (Intel Core 2 Duo, 3 GHz).

Table 1
Comparison of CPU time (sec.)

Newmark	HHT	Bi-First
27	32	15

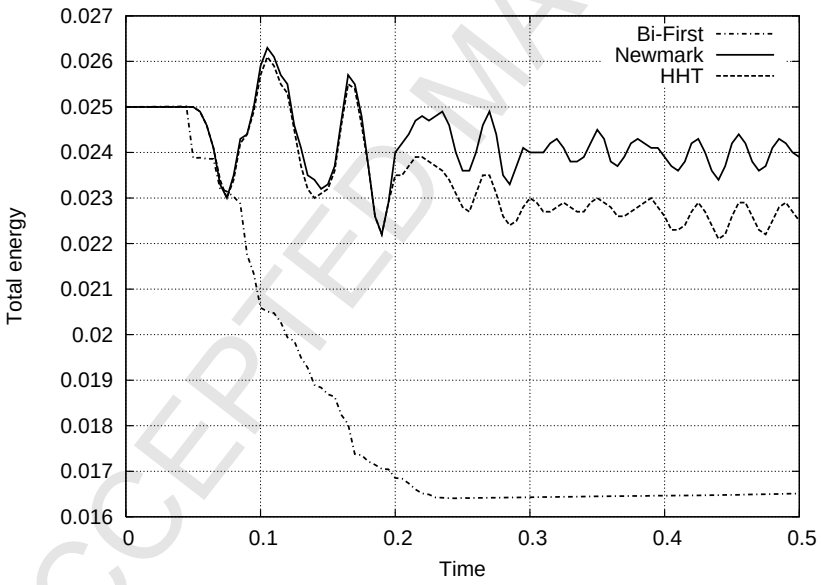

Fig. 17. Total energy with different methods

5 Conclusion

In this paper, we have proposed a finite element implementation of the Yeoh model and a numerical application to the case of large deformation con-

tact/impact with Coulomb friction between rigid and hyperelastic bodies. From numerical experiments, we have found that:

- The stress concentration is observed in the static contact problem.
- The total energy is well conserved for frictionless impact problem.
- The algorithm allows to determine quantitatively the physical energy dissipation by friction.
- The dissipated energy is not a monotonic function of the friction coefficient.
- The proposed Bi-First algorithm is more efficient and more stable than the Newmark and HHT algorithms.

References

[1] P. Wriggers. *Computational contact mechanics.* John Wiley & Sons, 2002.

[2] T. A. Laursen. *Computational contact and impact mechanics: Fundamentals of modeling interfacial phenomena in nonlinear finite element analysis.* Springer Verlag, 2002.

[3] G. de Saxcé and Z.-Q. Feng. The bi-potential method: a constructive approach to design the complete contact law with friction and improved numerical algorithms. *Mathematical and Computer Modeling*, 28(4-8):225–245, 1998.

[4] Z.-Q. Feng, F. Peyraut, and N. Labed. Solution of large deformation contact problems with friction between Blatz-Ko hyperelastic bodies. *Int. J. Engng. Science*, 41:2213–2225, 2003.

[5] H. M. Hilber, T. J. R. Hughes, and R. L. Taylor. Improved numerical dissipation for the time integration algorithms in structural dynamics. *Earthquake Engng. Struc. Dyn.*, 5:283–292, 1977.

[6] M. Jean. The non-smooth contact dynamics method. *Comp. Meth. Appl. Mech. Engng.*, 177:235–257, 1999.

[7] Z.-Q. Feng, B. Magnain, J.-M. Cros, and P. Joli. Energy dissipation by friction in dynamic multibody contact problems. In Z.-H. Yao, M.-W. Yuan, and W.-X. Zhong, editors, *Computational Mechanics*, Beijing, China, Sept. 2004. WCCM VI in conjunction with APCOM04, Springer.

[8] Z.-Q. Feng, P. Joli, J.-M. Cros, and B. Magnain. The bi-potential method applied to the modeling of dynamic problems with friction. *Comput. Mech.*, 36:375–383, 2005.

[9] P.J. Blatz and W.L. Ko. Application of finite elastic theory to the deformation of rubbery materials. *Transactions of the Society of Rheology*, 6:223–251, 1962.

[10] R.W. Ogden. *Non-linear elastic deformations.* Ellis Horwood, 1984.

[11] E.M. Arruda and M.C. Boyce. A three dimensional constitutive model for the large deformation stretch behavior of rubber elastic materials. *J. Mech. Phys. Solids*, 41:389–412, 1993.

[12] O.H. Yeoh. Some forms of the strain energy function for rubber. *Rubber Chem. Technol.*, 66:745–771, 1993.

[13] A.N. Gent. A new constitutive relation for rubber. *Rubber Chem. Technol.*, 69:59–61, 1996.

[14] J. C. Simo and T. J. R. Hughes. *Computational inelasticity.* Springer-Verlag, New York, 1998.

[15] C.O. Horgan and G. Saccomandi. Finite thermoelasticity with limiting chain extensibility. *J. Mech. Phys. Solids*, 51:1127–1146, 2003.

[16] J.M. Solberg and P. Papadopoulos. A finite element method for contact/impact. *Finite Elements in Analysis and Design*, 30:297–311, 1998.

[17] Z.-Q. Feng. 2D or 3D frictional contact algorithms and applications in a large deformation context. *Comm. Numer. Meth. Engng.*, 11:409–416, 1995.

[18] Z.-Q. Feng. http://lmee.univ-evry.fr/∼feng/FerImpact.html.

[19] K. Hofstetter, Ch. Grohs, J. Eberhardsteiner, and H.A. Mang. Sliding behaviour of simplified tire tread patterns investigated by means of FEM. *Computers & Structures*, 84:1151–1163, 2006.

[20] J. Chung and G. M. Hulbert. A time integration algorithm for structural dynamics with improved numerical dissipation: The generalized$-\alpha$ method. *Journal of Applied Mechanics, Transactions of the ASME*, 60:371–375, 1993.